ELSEVIER

Journal of Fluids and Structures 18 (2003) 613–633

JOURNAL OF FLUIDS AND STRUCTURES

www.elsevier.nl/locate/jnlabr/yjfls

Staggered circular cylinders immersed in a uniform planar shear flow

O.O. Akosile, D. Sumner*

Department of Mechanical Engineering, University of Saskatchewan, 57 Campus Drive Saskatoon, Saskatchewan, Canada S7N 5A9

Received 6 August 2002; accepted 11 July 2003

Abstract

Two circular cylinders of equal diameter, arranged in staggered configurations with dimensionless centre-to-centre pitch ratios of $P/D = 1.125$ and 1.25, were immersed in a uniform planar shear flow with a dimensionless shear parameter of $K = 0.05$ and a Reynolds number of $\mathrm{Re} = 5.0 \times 10^4$. The mean aerodynamic forces and the vortex shedding frequencies were measured for the upstream and downstream cylinders at each pitch ratio. Under uniform flow conditions, where there is no shear, the cylinders behave as a single bluff body with a single vortex shedding process. The aerodynamic force coefficients on both cylinders, and the Strouhal number, undergo complex changes as the incidence angle is varied from $\alpha = 0^\circ$ to 90°. At several critical incidence angles there are discontinuous changes in, or extreme values of, the aerodynamic force coefficients. These are related to the shear layer dynamics between the upstream and downstream cylinders at lower incidence angles, and the changes to the gap flow between the cylinders and the effect of base bleed at higher incidence angles. The effects of the uniform planar shear flow were mostly seen in the aerodynamic forces, particularly for the mean drag coefficient, where there was a reduction in drag for the upstream cylinder at all incidence angles, a reduction in drag for the downstream cylinder at higher incidence angles, small changes in the lift coefficient on the upstream cylinder, and shifts in the critical incidence angles. In contrast, the behaviour of the Strouhal number was generally unchanged, although a small reduction in Strouhal number was observed. Planar shear flow more strongly influenced the staggered cylinders at higher incidence angles, where it had an influence on the direction and strength of the gap flow, seen in the movement of two critical incidence angles, which was accompanied by a weakening of the vortex shedding process.

1. Introduction

A circular cylinder immersed in a uniform approach flow has been a well-studied problem in fluid mechanics. The cylinder experiences a high mean drag force coefficient and, for a wide range of Reynolds number, its flow field is characterized by the alternate, periodic shedding of Kármán vortices. The tendency towards vortex-induced vibration of the circular cylinder has been an important motivating factor for its study.

In many engineering applications, a cylindrical structure is immersed in a nonuniform approach flow, which may influence the vortex shedding behaviour and the aerodynamic forces. Examples include a circular cylinder immersed in a mixing layer (Kiya et al., 1979) or adjacent to a plane wall boundary (Price et al., 2002). The simplest case of a nonuniform approach flow is a uniform shear flow, where there is a linear variation of the approach flow velocity, yielding a constant velocity gradient and vorticity. Griffin (1985) has reviewed a number of experimental studies of

*Corresponding author. Tel.: +1-306-+966-5537; fax: +1-306-966-5427.
E-mail address: david.sumner@usask.ca (D. Sumner).

0889-9746/$ - see front matter © 2003 Elsevier Ltd. All rights reserved.
doi:10.1016/j.jfluidstructs.2003.07.014

Nomenclature

A	velocity gradient (s^{-1})
AR	cylinder aspect ratio
C_D	mean drag force coefficient
C_L	mean lift force coefficient
C_T	total mean aerodynamic force coefficient
D	diameter of cylinder (m)
F_D	mean drag force (N)
F_L	mean lift force (N)
f	frequency of vortex shedding (Hz)
K	shear parameter
L	length of cylinder (m)
P	centre-to-centre pitch or spacing (m)
Re	Reynolds number
St	Strouhal number
T	centre-to-centre transverse spacing (m)
U	approach velocity (m/s)
U_C	centre-line velocity (m/s)
$U_{C,d}$	centre-line velocity for the downstream cylinder (m/s)
$U_{C,u}$	centre-line velocity for the upstream cylinder (m/s)
x	streamwise direction (m)
y	cross-flow direction (m)
α	incidence angle (deg)
θ	direction of C_T with respect to the mean flow (deg)
ν	kinematic viscosity (m^2/s)
ρ	fluid density (kg/m^3)

two-dimensional bluff bodies in shear flow, including both stationary and oscillating cylinders. The study of a uniform shear flow is a common starting point for investigation of bluff bodies in more complex nonuniform approach flows.

In a planar shear flow, Fig. 1, the approach velocity, $U(y)$, varies across the diameter of the cylinder, D. This problem is applicable to undersea pipelines immersed in an ocean current or near the seabed, or to long-span bridges immersed in the atmospheric boundary layer, for example. The uniform planar shear flow velocity profile, $U(y)$, is given by

$$U(y) = U_C + Ay \tag{1}$$

for constant velocity gradient, $A(= \mathrm{d}U/\mathrm{d}y)$, cross-stream coordinate, y, and the centre-line value of the approach velocity, U_C (Fig. 1). The Reynolds number is based on the centre-line velocity, i.e. $\mathrm{Re} = U_C D/\nu$, where ν is the kinematic viscosity of the fluid. The velocity gradient of the uniform shear flow is characterized by a dimensionless shear parameter, $K = AD/U_C$. The shear parameter identifies a flow as having no shear ($K = 0$), low to moderate shear (K being small), or strong shear (K being large), although there is no commonly accepted definition of what constitutes low, moderate or strong shear.

Previous experimental studies have shown that a uniform planar shear flow causes the circular cylinder to experience a lower mean drag force than in a uniform flow (Adachi and Kato, 1975; Hayashi et al., 1991, 1993; Kwon et al., 1992; Sumner and Akosile, 2002); the mean drag force is represented by the dimensionless drag coefficient, $C_D(= 2F_D/\rho U_C^2 DL$, where F_D is the mean drag force, ρ is the fluid density, and L is the span of the cylinder). The shear flow also causes an asymmetric mean static pressure distribution on the surface of the cylinder, which results in a small steady mean lift force directed towards the low-velocity side (Adachi and Kato, 1975; Hayashi et al., 1991, 1993; Sumner and Akosile, 2002); the mean lift force is represented by the dimensionless lift coefficient, $C_L(= 2F_L/\rho U_C^2 DL$, where F_L is the mean lift force). Some selected results are given in Table 1. Concerning the vortex shedding frequency, lower Reynolds number experiments, $\mathrm{Re} = 35$–1600, have shown that a planar shear flow acts to increase the vortex shedding frequency compared to the no-shear case (Kiya et al., 1980b; Kwon et al., 1992). The vortex shedding frequency is represented in dimensionless form by the Strouhal number, $\mathrm{St}(= fD/U_C$, where f is the vortex shedding frequency). There have been few reported Strouhal number measurements at higher subcritical Reynolds numbers, i.e. $10^4 < \mathrm{Re} < 10^5$, however. For low-to-moderate shear, Sumner and Akosile (2002) instead found a small reduction in the

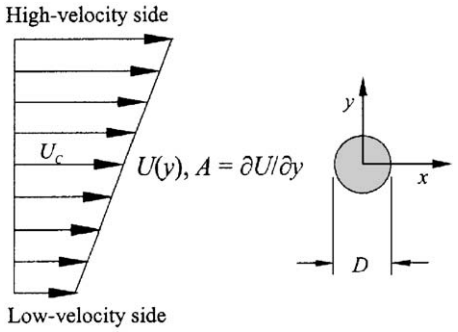

Fig. 1. A single, isolated circular cylinder in a uniform planar shear flow.

Table 1
Experimental results for a single, isolated circular cylinder in low to moderate uniform planar shear flow at higher subcritical Reynolds numbers

	Re	C_D	C_L	St
$K = 0$ (no shear)	5.0×10^4	1.22 ± 0.02	0.00 ± 0.02	0.193 ± 0.007
$K = 0.04$ (Adachi and Kato, 1975)	0.8×10^4	1.080	−0.037	N/A
$K = 0.05$ (Sumner and Akosile, 2002)	5.0×10^4	1.14 ± 0.02	-0.03 ± 0.02	0.188 ± 0.007
$K = 0.15$ (Hayashi et al., 1991)	6.0×10^4	0.997	−0.109	N/A

Strouhal number at higher subcritical Reynolds numbers, but the reduction fell within the uncertainty limits of their experiments; see Table 1. Overall, the effects of a planar shear flow on the circular cylinder are consistent with a narrowing, or reduction in width, of the near-wake region of the circular cylinder, compared to the no-shear case (Sumner and Akosile, 2002).

Groups of circular cylinders immersed in cross-flow arise in a number of engineering applications. Some of these include the designs for heat exchangers, cooling systems for nuclear power plants, offshore structures, buildings, chimneys, and power transmission lines. The most general arrangement of two circular cylinders of equal diameter is known as the staggered configuration, Fig. 2(a). The behaviour of the flow around two staggered cylinders, as well as the aerodynamic force coefficients and the vortex shedding frequencies, are highly dependent on the dimensionless centre-to-centre pitch ratio, P/D, and the incidence angle, α (Cooper, 1974; Zdravkovich and Pridden, 1977; Kiya et al., 1980a; Sumner et al., 2000; Sumner and Richards, 2002, 2003a, b).

The effects of a uniform planar shear flow on multiple cylinders have not been extensively studied. For two staggered cylinders, the upstream and downstream cylinders will experience different centre-line velocities, $U_{C,u}$ and $U_{C,d}$, where the subscripts u and d refer to the upstream and downstream cylinders, respectively. The effect of shear will therefore be different depending on whether the downstream cylinder is situated at a higher centre-line velocity, $U_{C,d} > U_{C,u}$ (Fig. 2(b)), or a lower centre-line velocity, $U_{C,d} < U_{C,u}$ (Fig. 2(c)), than the upstream cylinder. In one of the few studies of a cylinder group in a planar shear flow, El-Taher (1984) examined two equal-diameter circular cylinders in the side-by-side configuration (corresponding to $\alpha = 90°$) with $K = 0.02$, which corresponded to a flow with low shear. The shear flow was found to have a small influence on the critical values of P/D at which the flow transitioned from one steady flow pattern to another, compared to the no-shear case.

In the present study, the effect of a uniform planar shear flow on the staggered configuration of two circular cylinders of equal diameter was examined experimentally. Staggered configurations of $P/D = 1.125$ and 1.25 were tested at $\mathrm{Re} = 5.0 \times 10^4$, in both a uniform freestream, $K = 0$, and in a uniform planar shear flow, with $K = 0.05$.

2. Experimental set-up and procedure

The experiments were conducted in a low-speed, closed-return wind tunnel, with a test section of 0.91 m (height) × 1.13 m (width) × 1.96 m (length). A ground plane was installed near the test section floor. Details of the experimental set-up are shown in Fig. 3. Under uniform flow conditions, the longitudinal freestream turbulence

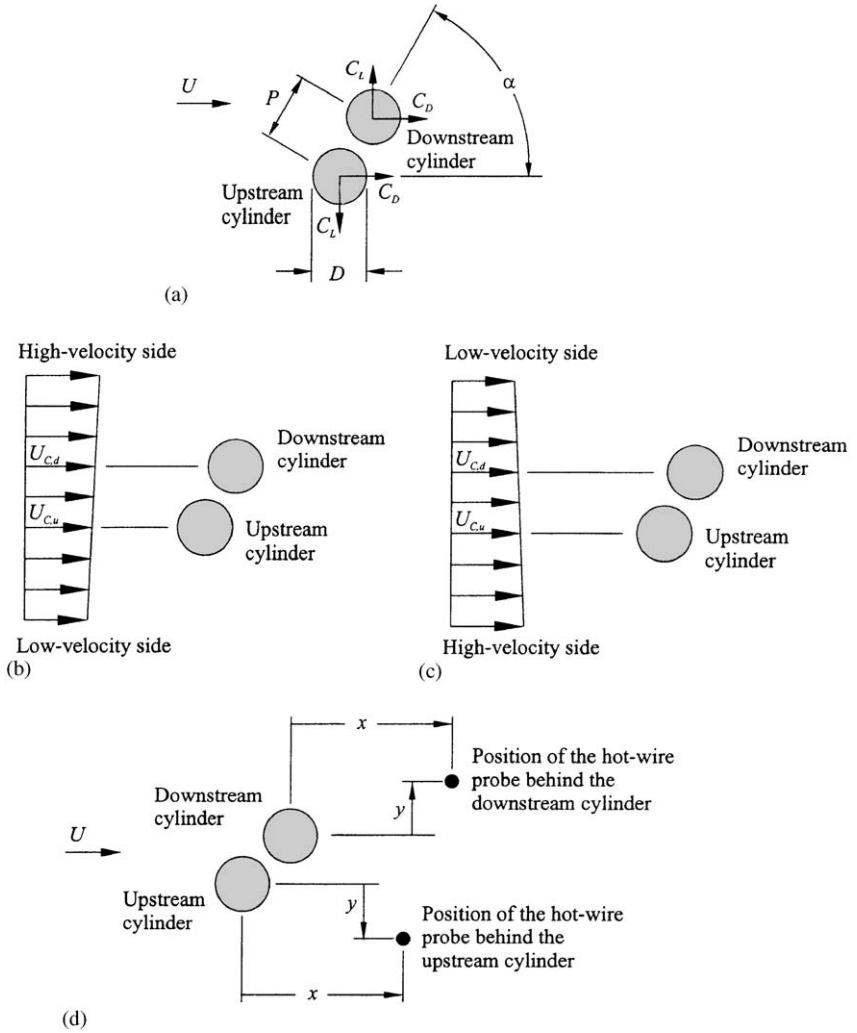

Fig. 2. Staggered circular cylinders of equal diameter in cross-flow ($P/D = 1.25$ shown): (a) uniform flow, showing the force convention for the upstream and downstream cylinders; (b) uniform planar shear flow ($K = 0.05$ shown), with the downstream cylinder at a higher centre-line velocity than the upstream cylinder, $U_{C,d} > U_{C,u}$; (c) uniform planar shear flow ($K = 0.05$ shown), with the downstream cylinder at a lower centre-line velocity than the upstream cylinder, $U_{C,d} < U_{C,u}$ and (d) position of the hot-wire probe relative to the upstream and downstream cylinders ($x/D = 3.0$, $y/D = 1.0$ shown).

intensity was 0.6% and the velocity nonuniformity in the central portion of the test section, outside the test section wall boundary layers, was 0.5%.

To generate a uniform shear flow, a contoured honeycomb was installed at the entrance to the test section, immediately downstream of the contraction; see Fig. 3(a). The shape of the honeycomb was designed using the method of Kotansky (1966) to achieve the desired velocity gradient. Some fine-tuning of the honeycomb shape was necessary to ensure a smooth velocity profile, Fig. 4, which was uniform to within 2.4%. The longitudinal freestream turbulence intensity was less than 1.5% downstream of honeycomb. Further details about the design of the shear flow generator are given in Akosile and Sumner (2001), Akosile (2002), and Sumner and Akosile (2002).

Two circular cylinders of equal diameter, $D = 0.032$ m, were arranged in staggered configurations of $P/D = 1.125$ and 1.25, similar to that adopted by Sumner and Richards (2002, 2003a, b). The cylinders were tested in the higher subcritical Reynolds number regime, at $\mathrm{Re} = 5.0 \times 10^4$. The first cylinder was mounted vertically from a six-component force balance located outside and below the wind tunnel test section, referred to as the central cylinder in Fig. 3(a). This cylinder was centrally located in the test section. The second cylinder was mounted between a pair of circular end plates, referred to as the outer cylinder in Fig. 3(a); details of the end plate design are shown in Fig. 3(b). The end plate design

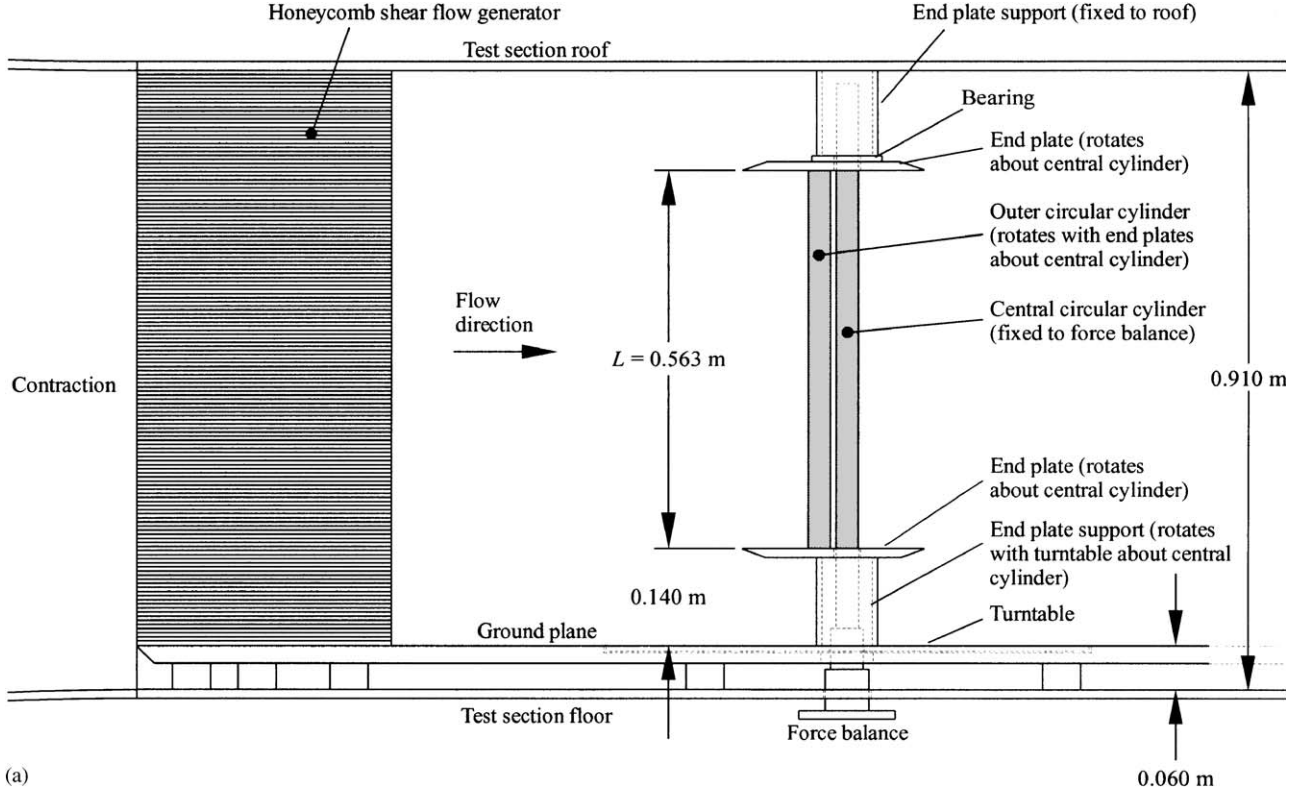

Fig. 3. (a) Experimental set-up in the wind tunnel, $P/D = 1.25$ and (b) detail of end plates and end plate supports.

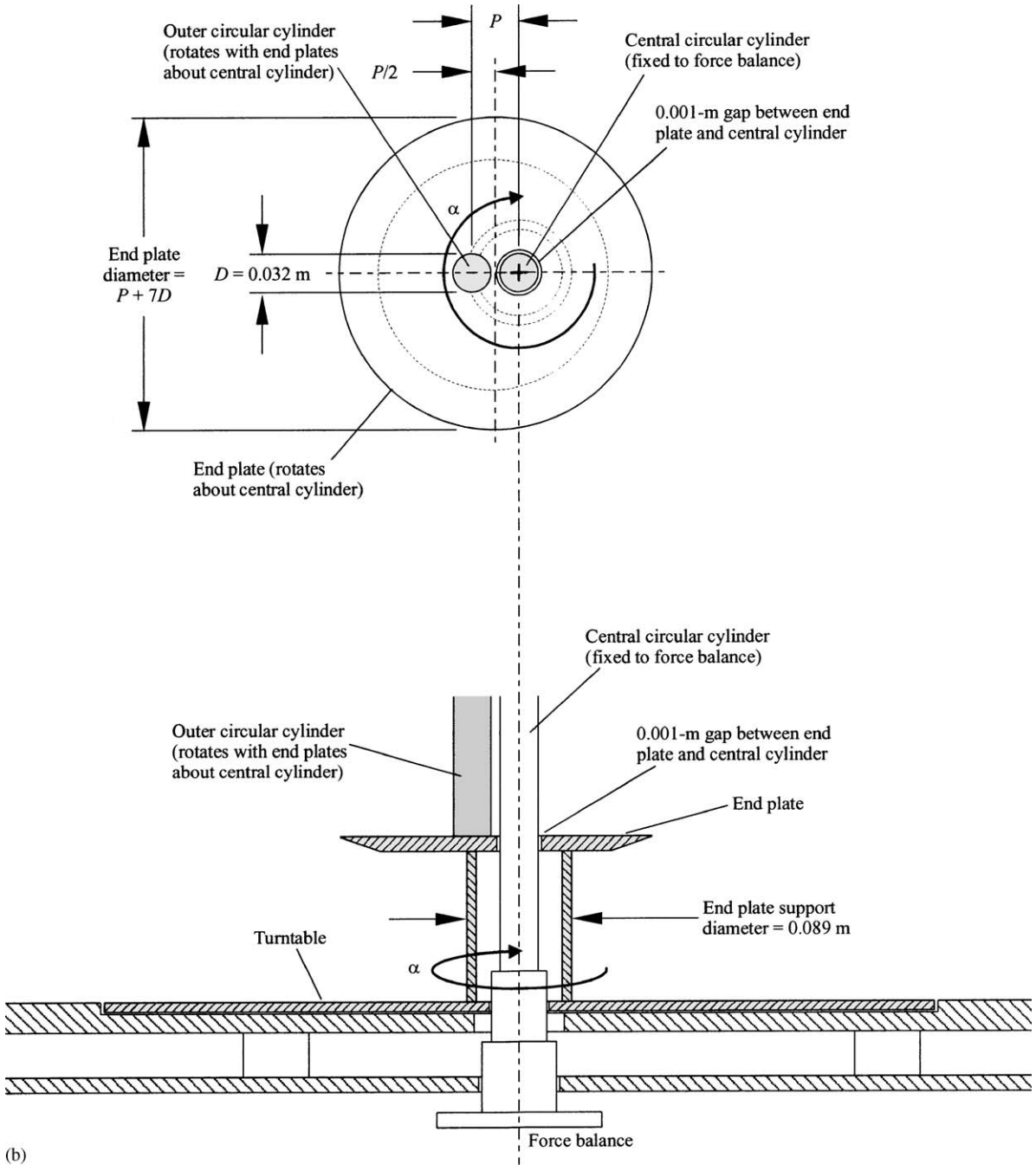

Fig. 3 (*continued*).

was similar to that adopted by Sumner et al. (2000), and was based on the recommendations of Szepessy (1993), with an overall diameter of $P + 7D$. The end plates were positioned away from the test section roof and ground plane on cylindrical supports, as shown in Fig. 3(a), so that the cylinders were located outside the boundary layers developing on these surfaces.

The outer cylinder, end plates, and end plate supports could be rotated in α about the central cylinder using a computer-controlled turntable imbedded in the ground plane; see Fig. 3(b). In this way, the central cylinder could represent either an upstream or downstream cylinder, over the full range of incidence angle, $\alpha = 0-90^{\circ}$. The

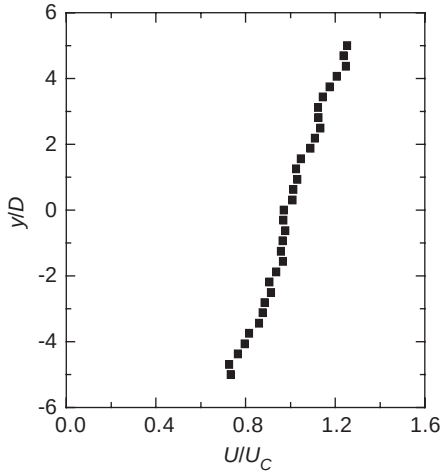

Fig. 4. Uniform shear velocity profile 0.6 m downstream of the shear flow generator, at the test section centre-line, $U_C = 24.3\,\mathrm{m/s}$, $A = 36.7\,\mathrm{s}^{-1}$, $K = 0.05$, nonuniformity of 2.4%.

uncertainty in angular position was estimated at $\pm 0.25^\circ$. The central cylinder was isolated from the outer cylinder and its end plates by a 1-mm gap, as shown in Fig. 3(b). The cylindrical end plate supports surrounded the central cylinder and shielded it from the oncoming flow, see Fig. 3(b), meaning the length of each cylinder that was exposed to the flow was the same, $L = 0.563\,\mathrm{m}$, giving an aspect ratio of $\mathrm{AR} = L/D = 17.6$ and a solid blockage ratio of 1.75% per cylinder; see Fig. 3(a).

Reference flow conditions were measured with a Pitot-static probe (United Sensor, 3.2-mm diameter) and Datametrics Barocell absolute and differential pressure transducers. Vortex shedding frequencies were measured with a single-sensor hot-wire probe (TSI Model 1210-T1.5) and a TSI IFA-100 constant temperature anemometer. The probe was positioned at mid-span and downstream of the cylinder of interest, at $x/D = 3.0$ and $y/D = 1.0$, using a three-axis computer-controlled traversing system. The position of the hot-wire probe is shown in Fig. 2(d). Data were acquired with a Pentium II microcomputer, a National Instruments AT-MIO-64F-5 12-bit multifunction board and LabVIEW software. The measurement uncertainty of the mean lift and drag coefficients was estimated at $C_L \pm 0.02$ and $C_D \pm 0.02$. The measurement uncertainty of the Strouhal number was estimated at $\mathrm{St} \pm 0.007$.

The staggered cylinder experiments for $P/D = 1.125$ and 1.25, and $\alpha = 0-90^\circ$, were conducted at $\mathrm{Re} = 5.0 \times 10^4$ and a shear parameter of $K = 0.05$. In each case, the mean aerodynamic forces and the vortex shedding frequencies were measured for both the upstream and downstream cylinders, for small increments of α, varying from 1° to 5°.

3. Results and discussion—uniform flow

Under uniform flow conditions (no shear, $K = 0$), the flow field for staggered cylinder configurations of $P/D = 1.125$ and 1.25 is similar to a single bluff body for nearly the entire range of α, since the cylinders are situated very close to one another and the gap between them is small (Sumner et al., 2000). At these small pitch ratios, Kármán vortex shedding tends to occur from the cylinder group as a whole, rather than from the individual cylinders, and there is single Kármán vortex street in the combined wake. Representative flow patterns are shown in Fig. 5. In a tandem configuration, $\alpha = 0^\circ$, the shear layers from the upstream cylinder wrap around and enclose the downstream cylinder. As the incidence angle is increased, $\alpha = 15^\circ$ and 30°, the inner shear layer from the upstream cylinder either wraps around, or reattaches onto, the downstream cylinder. At larger incidence angles, $\alpha = 60^\circ$, shear layer reattachment onto the downstream cylinder can no longer be maintained. Instead, some of the approach flow is directed through the gap between the cylinders and enters the near-wake region. This weak gap flow is similar to "base bleed," which refers to the injection of low-momentum fluid into the near-wake of a bluff body. Some of the effects of base bleed include an increase in the vortex formation length, a reduction in drag force, and a weakening of the Kármán vortex shedding process (Bearman, 1967; Wood, 1967). For two staggered cylinders, the direction and strength of the gap flow vary with the incidence angle, being either deflected towards the upstream cylinder or the downstream cylinder, or being directed along the flow centre-line (Sumner et al., 2000). In the side-by-side configuration, $\alpha = 90^\circ$, the two cylinders continue to behave as if a

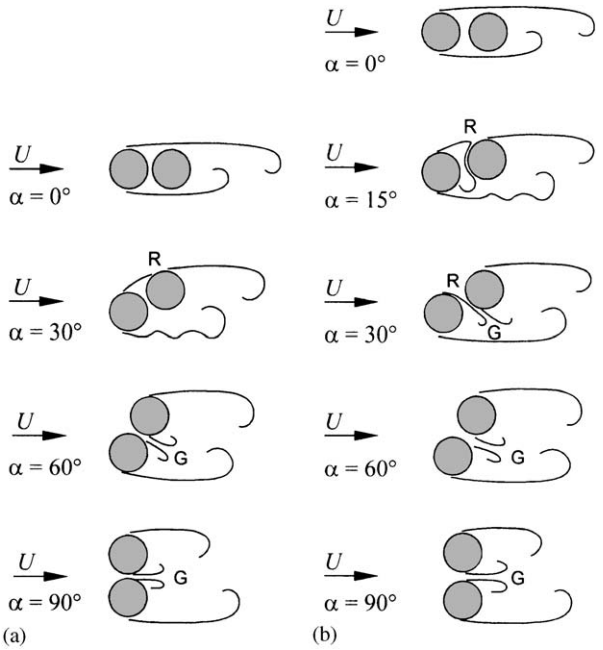

Fig. 5. Flow patterns for two closely spaced staggered cylinders in uniform flow (no shear, $K = 0$), based on Sumner et al. (2000): (a) $P/D = 1.125$; (b) $P/D = 1.25$. R = shear layer reattachment, G = gap flow.

single bluff body with "base bleed" (Sumner et al., 1999). Further details of the flow patterns are given by Sumner et al. (1999, 2000).

There are few sets of aerodynamic force data reported in the literature for staggered cylinders with very small pitch ratios, and few sets of data for the upstream cylinder (Sumner and Richards, 2002). Therefore, initial experiments with the staggered cylinders were conducted without the shear flow generator installed in the wind tunnel, to obtain data under uniform flow conditions, $K = 0$, for comparison purposes. Similar experiments, with and without the shear flow generator installed, were also conducted for a single, isolated circular cylinder; these results are reported by Akosile (2002) and Sumner and Akosile (2002).

The aerodynamic force data for the staggered cylinders in uniform flow (no shear, $K = 0$) are shown in Figs. 6 and 7, for $P/D = 1.125$ and 1.25, respectively. Here, an outward-directed lift force on a cylinder is considered positive, and an inward-directed lift force on a cylinder is considered negative (Fig. 2(a)). For both pitch ratios, the results for the downstream cylinder are in good agreement with the data of Cooper (1974). The Strouhal number data for the two configurations are shown in Fig. 8 and selected power spectra are shown in Fig. 9.

3.1. Forces on the upstream cylinder

The behaviour of the mean aerodynamic force coefficients with incidence angle, for the upstream cylinder, is mostly similar for the two pitch ratios (Figs. 6(a) and 7(a)). The lift force on the upstream cylinder experiences large changes in magnitude, and it may be either inward-directed (negative) or outward-directed (positive). The drag force on the upstream cylinder may be up to 30% higher (unfavourable) or 25% lower (favourable) than the value for a single, isolated circular cylinder, depending on the incidence angle.

Apart from these basic trends in the force data, there are four critical incidence angles, denoted by A, B, C, D in Figs. 6(a) and 7(a), which correspond to discontinuous changes in, or local maximum or minimum values of, the mean aerodynamic force coefficients on the upstream cylinder. A fifth critical incidence angle, denoted E′ in Fig. 6(b), occurs for the downstream cylinder at $P/D = 1.125$ only, and is discussed in Section 3.2.

In the tandem configuration, $\alpha = 0^\circ$, there is zero mean lift force on the upstream cylinder and the mean drag coefficient is close to the value for a single, isolated circular cylinder.

For $\alpha < 20^\circ$ at $P/D = 1.125$ (Fig. 6(a)), and for $\alpha < 32^\circ$ at $P/D = 1.25$ (Fig. 7(a)), the lift force on the upstream cylinder is inward-directed (negative), which means that the upstream cylinder is pulled towards the downstream cylinder. Also, the drag force on the upstream cylinder remains lower than that of a single cylinder (Figs. 6(a) and 7(a)).

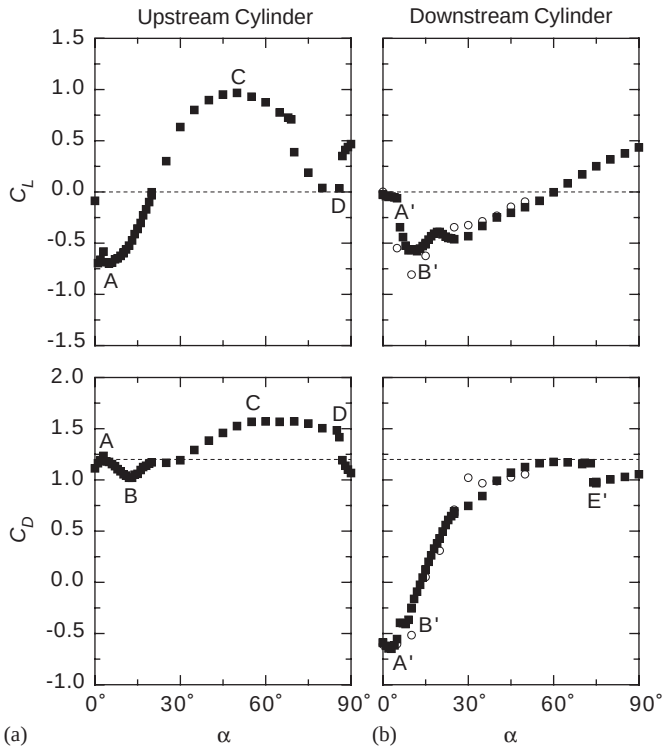

Fig. 6. Aerodynamic force coefficients for a staggered configuration of $P/D = 1.125$ in uniform flow (no shear, $K = 0$), $\mathrm{Re} = 5.0 \times 10^4$: (a) upstream cylinder; (b) downstream cylinder. Critical incidence angles identified as A, B, C, D, A′, B′, E′. ○, Cooper (1974), $\mathrm{Re} = 4.95 \times 10^4$; - - -, single, isolated circular cylinder.

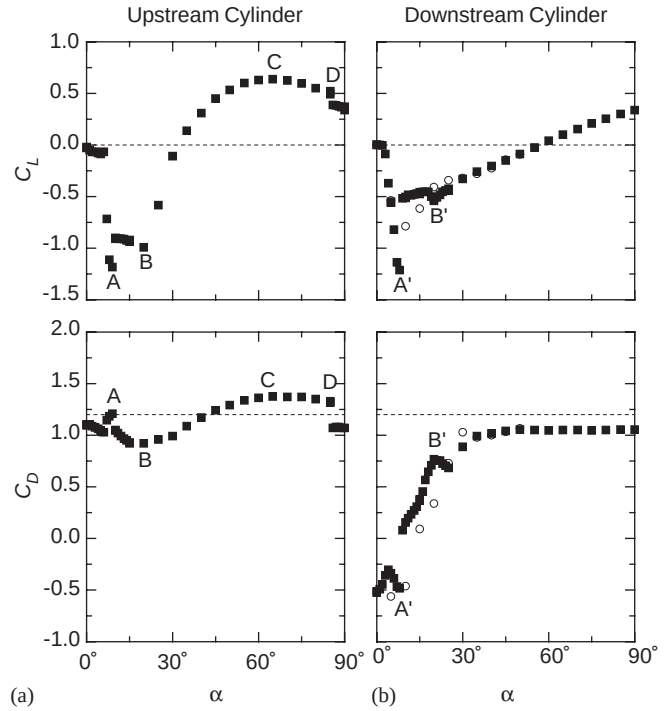

Fig. 7. Aerodynamic force coefficients for a staggered configuration of $P/D = 1.25$ in uniform flow (no shear, $K = 0$), $\mathrm{Re} = 5.0 \times 10^4$: (a) upstream cylinder; (b) downstream cylinder. Critical incidence angles identified as A, B, C, D, A′, B′. ○, Cooper (1974), $\mathrm{Re} = 4.95 \times 10^4$; - - -, single, isolated circular cylinder.

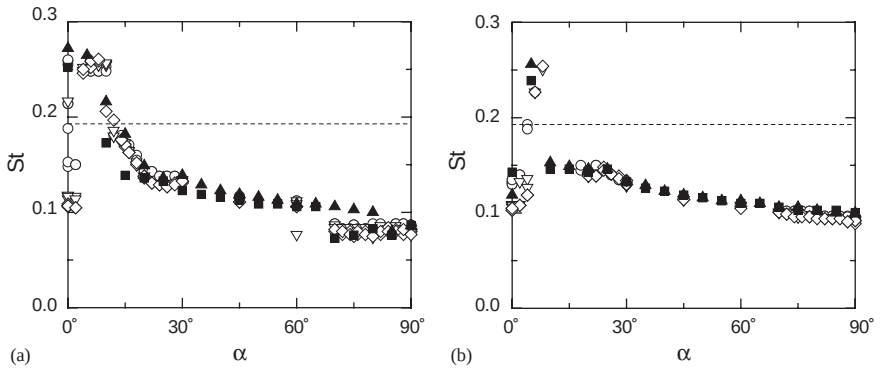

Fig. 8. Strouhal number data for staggered cylinder configurations in uniform flow (no shear, $K = 0$), $\mathrm{Re} = 5.0 \times 10^4$: (a) $P/D = 1.125$; (b) $P/D = 1.25$. ■, upstream cylinder; ▲, downstream cylinder; - - - single, isolated circular cylinder. Data from Sumner and Richards (2003b): ○, $\mathrm{Re} = 3.2 \times 10^4$; ▽, $\mathrm{Re} = 5.6 \times 10^4$; ◇, $\mathrm{Re} = 7.4 \times 10^4$.

It is in this range of α that the shear layer from the upstream cylinder either wraps around, or reattaches onto, the downstream cylinder (Fig. 5). Two critical incidence angles are found in this range of α. The first critical incidence angle, A, occurs at $\alpha \approx 5^\circ$ for both pitch ratios (Figs. 6(a) and 7(a)), where there is a local minimum value of the inward-directed lift force and a local maximum value of the drag force. The second critical incidence angle, B, occurs at $\alpha \approx 12^\circ$ for $P/D = 1.125$ (Fig. 6(a)) and $\alpha \approx 20^\circ$ for $P/D = 1.25$ (Fig. 7(a)), where there is a local minimum value for the drag coefficient. For $P/D = 1.25$ only (Fig. 7(a)), there is also a discontinuity in the lift coefficient at B. These critical incidence angles are associated with changes to the behaviour of the inner shear layer from the upstream cylinder, and its interaction with the downstream cylinder.

For $\alpha > 20^\circ$ at $P/D = 1.125$ (Fig. 6(a)), and for $\alpha > 32^\circ$ at $P/D = 1.25$ (Fig. 7(a)), the lift force on the upstream cylinder is outward-directed (positive), which means that the upstream cylinder is being pushed away from the downstream cylinder. For these α, shear layer reattachment can no longer be maintained; rather, the approach flow is increasingly directed through the gap between the cylinders (Fig. 5). At $\alpha = 30^\circ$ and 45°, for $P/D = 1.125$ and 1.25, respectively, the drag coefficient of the upstream cylinder becomes higher than a single circular cylinder (Figs. 6(a) and 7(a)). Within this large range of α is the third critical incidence angle, C, which corresponds to the maximum outward-directed lift force and the maximum drag force experienced by the upstream cylinder, at $\alpha \approx 50-60^\circ$ for $P/D = 1.125$ (Fig. 6(a)) and $\alpha \approx 65^\circ$ for $P/D = 1.25$ (Fig. 7(a)).

In the side-by-side configuration, $\alpha = 90^\circ$, the upstream cylinder continues to experience the repulsive lift force. However, the drag coefficient becomes lower than the value for a single, isolated circular cylinder (Figs. 6(a) and 7(a)), which may be attributed to the base-bleed effect of the gap flow. This reduction in drag is associated with the fourth critical incidence angle, D, which occurs at $\alpha \approx 86^\circ$ for both pitch ratios (Figs. 6(a) and 7(a)). Here, there is a discontinuous change in the lift and drag forces on the upstream cylinder, which suggests a sudden change in the behaviour of the base-bleed effect as α is increased. This may be attributed to a sudden increase in the strength of the gap flow, or a change in the deflection angle of the gap flow (see also the discussion of critical point E′, in Section 3.2). A biased base-bleed flow has been observed for closely spaced side-by-side cylinders (Sumner et al., 1999) and staggered cylinders (Sumner et al., 2000). This flow pattern is distinct from the more familiar biased flow pattern for the side-by-side configuration, however, which occurs at much higher pitch ratios and has two Kármán vortex shedding processes, one occurring from each cylinder.

3.2. Forces on the downstream cylinder

Similar to the upstream cylinder, the behaviour of the mean aerodynamic force coefficients with incidence angle on the downstream cylinder is mostly the same for the two pitch ratios (Figs. 6(b) and 7(b)). The lift force on the downstream cylinder is strongly inward-directed (negative) at lower incidence angles, but becomes outward-directed (positive) at higher incidence angles. The drag force on the downstream cylinder remains similar to, or lower than, the value for a single, isolated circular cylinder. At small incidence angles, the drag force is negative, indicating that a thrust force acts upon the downstream cylinder.

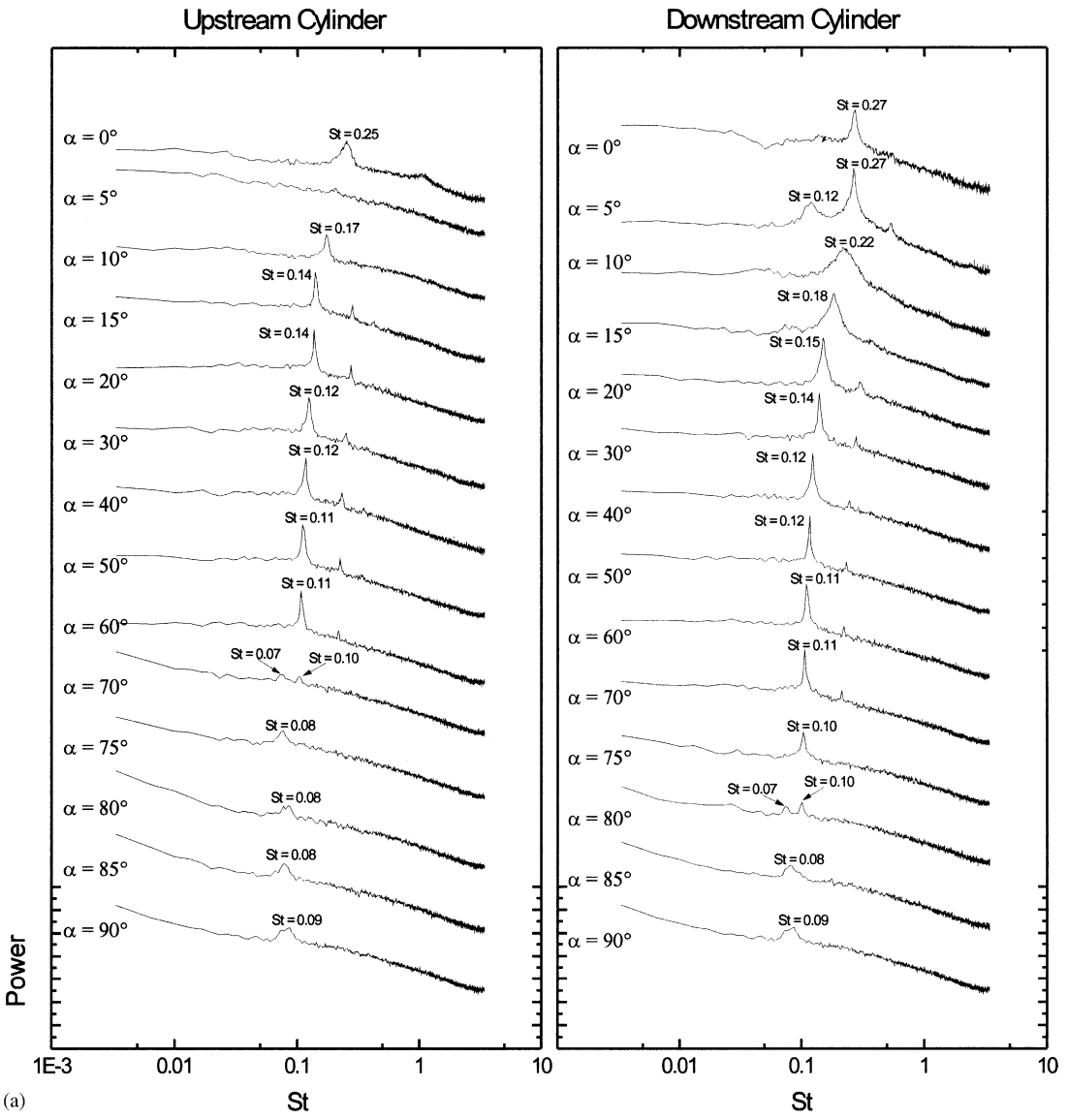

Fig. 9. Selected power spectra, as a function of incidence angle, measured behind the upstream and downstream cylinders, uniform flow (no shear, $K = 0$), $\mathrm{Re} = 5.0 \times 10^4$, corresponding to the Strouhal number data in Fig. 8: (a) $P/D = 1.125$; (b) $P/D = 1.25$. Each spectrum represents 250 averages. The vertical scale is arbitrary, but the same scale is used for each spectrum.

Three critical incidence angles, denoted by A′, B′ and E′, are identified in Figs. 6(b) and 7(b), where the "prime" refers to the downstream cylinder. Two of these critical angles, A′ and B′, directly correspond to those identified for the upstream cylinder, A and B (Figs. 6(a) and 7(a)). The latter angle, E′, is unique to the downstream cylinder for $P/D = 1.125$ (Fig. 6(b)).

In the tandem configuration, $\alpha = 0^\circ$, the lift force on the downstream cylinder is zero and the drag force is negative, for both pitch ratios (Figs. 6(b) and 7(b)). The downstream cylinder is completely enclosed by the shear layers from the upstream cylinder (Fig. 5), and the resulting pressure distribution causes the downstream cylinder to experience a thrust force.

For small incidence angles, where the cylinders are nearly in tandem, there is a complex behaviour of the aerodynamic force coefficients that is associated with the tendency towards shear layer reattachment, from the upstream cylinder onto the downstream cylinder, and its eventual loss as α is increased (Fig. 5). Where the cylinders are

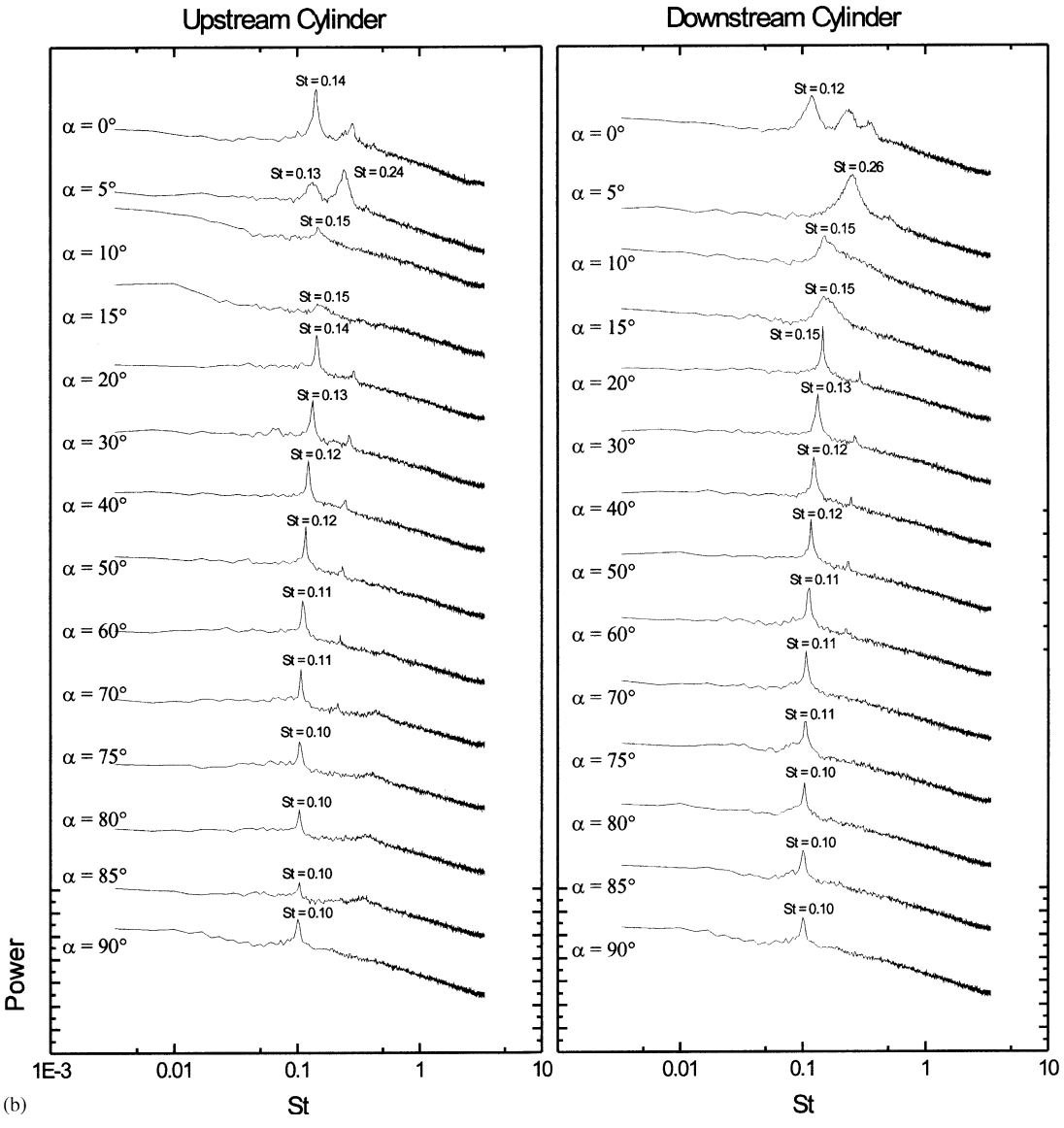

Fig. 9 (*continued*).

nearly tandem, the drag force on the downstream cylinder remains negative (Figs. 6(b) and 7(b)). This thrust force acts to pull the downstream cylinder into the near-wake region of the upstream cylinder. The drag force increases with the incidence angle, with zero drag force experienced at $\alpha \approx 13^\circ$ and $\alpha \approx 8^\circ$ for $P/D = 1.125$ and $P/D = 1.25$, respectively (Figs. 6(b) and 7(b)). Thereafter, the drag force remains positive for further increases in the incidence angle.

Two critical incidence angles, A′ and B′, are found in this range of α. The first critical angle, A′, denotes the sudden appearance of the maximum inward-directed (negative) lift force experienced by the downstream cylinder. The discontinuous behaviour at A′, and the maximum (negative) value of lift thereafter, is known as the "inner lift peak" (Zdravkovich and Pridden, 1977), and marks a sudden change in the behaviour of the inner shear layer from the upstream cylinder. The "inner lift peak" also coincides with a local minimum value for the drag coefficient (Zdravkovich and Pridden, 1977). The second critical angle, B′, denotes a local minimum value of the lift force, or local maximum value of the drag force. It too is associated with further changes in the reattachment region between the cylinders.

For $\alpha > 60^\circ$, the lift force on the downstream cylinder becomes positive, or outward-directed, meaning the downstream cylinder tends to be repelled away from the upstream cylinder (Figs. 6(b) and 7(b)). At high α, the drag coefficient for the downstream cylinder remains mostly lower than the value for a single, isolated circular cylinder, which may be attributed to the base-bleed phenomenon of the gap flow. It is in this range of α that the third critical incidence angle, E′, is found, at $\alpha \approx 73^\circ$, for $P/D = 1.125$ only (Fig. 6(b)). Here, there is a sudden drop in the drag coefficient with increasing α, which is absent from the lift coefficient data and from the data for the upstream cylinder. This critical incidence angle, E′, may also be caused by a change in the direction of the gap flow in the combined wake of the cylinders, which was observed by Sumner et al. (2000) at $\alpha = 60-75^\circ$. Initially, the gap flow is directed towards the upstream cylinder, but with an increase in the incidence angle, it becomes progressively more deflected towards the downstream cylinder instead. With more of the gap flow entering the base region of the downstream cylinder, there is an increase in the base pressure and a subsequent reduction in drag.

3.3. Strouhal number

The Strouhal number data for $P/D = 1.125$ and 1.25 are given in Fig. 8. The Strouhal data compare favourably with those of Sumner and Richards (2003b), which were acquired with much smaller increments in the incidence angle than the present study. The general behaviour of the data shows that the Strouhal numbers measured behind the upstream and downstream cylinders are nearly the same, which indicates that a single vortex shedding process was present. The detection of a single Strouhal number is consistent with the closely spaced cylinders behaving as a single bluff body (Sumner et al., 2000), as shown by the flow patterns in Fig. 5. In staggered configurations with higher pitch ratios than in the present study, two distinct Strouhal numbers are measured at most incidence angles, where the cylinders no longer behave as a single bluff body (Kiya et al., 1980a; Sumner et al., 2000; Sumner and Richards, 2003a, b).

As seen in Figs. 8a and b, the Strouhal number generally remains lower than that of a single, isolated circular cylinder for nearly the entire range of α. The Strouhal number steadily decreases with α to a value of $St \approx 0.1$ (one-half the vortex shedding frequency for an isolated circular cylinder). The lowering of the Strouhal number occurs as the near-wake region lengthens and widens with increasing α. In the nearly tandem configuration, $\alpha < 15^\circ$, the Strouhal number is higher than a single cylinder. The high frequencies measured at small incidence angles are also found in the tandem configuration (Ljungkrona et al., 1991), and are caused by a shortening and narrowing of the near-wake region compared to the case of a single cylinder (Sumner et al., 2000).

There is some degree of scatter in the St data at small incidence angles when the cylinders are nearly tandem. The reason for this scatter is apparent from the power spectra, Fig. 9, which show that the vortex shedding peaks are small and broad-banded when $\alpha < 20^\circ$. For $P/D = 1.125$, Fig. 9(a), there was no discernible vortex shedding frequency behind the upstream cylinder at $\alpha = 5^\circ$; for $P/D = 1.25$, Fig. 9(b), very small vortex shedding peaks were measured behind the upstream cylinder at $\alpha = 10^\circ$ and 15°. Within this same range of α, there were marked changes in the aerodynamic force coefficients also (Figs. 6 and 7). This relationship between the behaviour of the Strouhal number and the behaviour of the aerodynamic force coefficients has also been observed for staggered configurations with higher pitch ratios, and is attributed to the dynamics of the shear layer reattachment process (Sumner and Richards, 2003a).

For $P/D = 1.125$ (Fig. 8(a)), there are two discontinuities in the Strouhal number at incidence angles of $\alpha \approx 70^\circ$ and 80°, which broadly correspond to critical incidence angles E′ and D, respectively, seen in the behaviour of the aerodynamic force coefficients (Fig. 6). Specifically, as the incidence angle is increased there is a small reduction in the Strouhal number at $\alpha \approx 70^\circ$. At this critical incidence angle, there is also a change in the power spectra for $P/D = 1.125$ (Fig. 9(a)). The peaks for the upstream and downstream cylinders become noticeably smaller and more broad-banded for $\alpha > 60^\circ$. This behaviour of the power spectra is not seen at the larger pitch ratio, $P/D = 1.25$, (Fig. 9(b)), where critical incidence angle E′ is absent. Again, these critical incidence angles are thought to be related to the changes in the deflection and strength of the gap flow within the combined wake of the cylinders, and therefore would be expected to have an impact on the vortex shedding activity also. This lowering of the Strouhal number may be attributed to an enlargement of the near-wake region, which is one of the effects of base bleed. The reduction in the strength of the vortex shedding signal, indicated by the smaller and more broad-banded peak, also shows an effect of base bleed, which tends to weaken the vortex shedding mechanism.

A closer look at the power spectra for $P/D = 1.125$ (Fig. 9(a)) shows that two small vortex shedding peaks are measured for the upstream cylinder at $\alpha = 70^\circ$ and for the downstream cylinder at $\alpha = 80^\circ$. The lower peak, $St = 0.07$, corresponds to the base-bleed flow pattern when the cylinders are nearly side-by-side, while the higher peak, $St = 0.10$, corresponds to the flow pattern at intermediate incidence angles. The simultaneous appearance of the two peaks suggests that the two flow patterns may appear alternately, i.e. intermittently switch from one flow pattern to the other, on or about the critical incidence angle. Since it was not possible to measure the fluctuating forces on the cylinders, this bistable behaviour could not be observed in the aerodynamic forces.

4. Results and discussion—shear flow

Results for a single, isolated circular cylinder in a uniform planar shear flow have been reported previously by Akosile (2002) and Sumner and Akosile (2002), for $Re = 4.0 \times 10^4$–9.0×10^4 and $K = 0.02-0.07$. The single-cylinder results for $Re = 5.0 \times 10^4$ and $K = 0.05$ from Sumner and Akosile (2002), which used the same uniform planar shear flow conditions as the present study, were given in Table 1 alongside some selected previously published results. The results show a reduction in the mean drag coefficient (a 7% reduction in the study by Sumner and Akosile, 2002), the appearance of a small mean lift coefficient directed towards the low-velocity side (indicated by the negative sign, see Fig. 1), and a small reduction in the Strouhal number (but which falls within the limits of the experimental uncertainty).

For the staggered-cylinder configurations in shear flow, with $Re = 5.0 \times 10^4$ and $K = 0.05$, the aerodynamic force data are shown in Figs. 10 and 11, for $P/D = 1.125$ and 1.25, respectively. Data for a single, isolated circular cylinder, with and without shear, and data for the staggered cylinders without shear, are also shown in Figs. 10 and 11 for comparison purposes. Strouhal number data for the staggered cylinders in a shear flow are shown in Fig. 12 and selected power spectra are shown in Fig. 13.

4.1. Forces on the upstream cylinder

For the upstream cylinder (Figs. 10(a) and 11(a)), the influence of the uniform planar shear flow is more strongly seen for the mean drag coefficient, for both pitch ratios. The shear flow causes a reduction in drag coefficient at all incidence angles, with the reduction being more pronounced at higher incidence angles, as the cylinders more closely approximate the side-by-side configuration. At critical incidence angle C, where the upstream cylinder reaches its maximum lift and drag coefficients, the shear flow causes a reduction in the maximum mean drag coefficient of up to 22% for $P/D = 1.125$ (Fig. 10(a)) and of up to 17% for $P/D = 1.25$ (Fig. 11(a)). A single, isolated circular cylinder in a planar shear flow also experiences a reduction in the mean drag coefficient (Table 1), however the reduction is more pronounced for multiple cylinders.

The reduction in drag is mostly independent of whether one centre-line velocity, $U_{C,d}$ or $U_{C,u}$ (see Figs. 2b and c), is greater or less than the other, except in the neighbourhood of critical incidence angle D. For more closely spaced cylinders, $P/D = 1.125$ (Fig. 10(a)), critical angle D shifts from $\alpha \approx 86^\circ$ to 80° for $U_{C,d} > U_{C,u}$, whereas the discontinuity at D disappears for $U_{C,d} < U_{C,u}$. This same shift or disappearance for critical incidence angle D is seen in the lift coefficient data also. This critical incidence angle is linked with changes in the direction or strength of the gap flow entering the base region of the cylinders.

Apart from the changes in critical incidence angle D, the lift coefficient data for the upstream cylinder are mostly unchanged in the planar shear flow. However, the upstream cylinder experiences a small reduction in the lift coefficient when $U_{C,d} < U_{C,u}$ (Fig. 2(c)), at higher incidence angles, once the lift has become outward-directed (positive) (Figs. 10(a) and 11(a)). Since the upstream cylinder is fully exposed to the planar shear flow, it will experience a small inward-directed lift force similar to the single, isolated circular cylinder in a shear flow, which, in turn, causes the small reduction in lift force.

At lower incidence angles, where the inner shear layer from the upstream cylinder interacts strongly with the downstream cylinder, the effects of shear flow were more apparent for $P/D = 1.125$ (Fig. 10(a)), with the movement of critical angle B, corresponding to a local drag minimum, from $\alpha \approx 12^\circ$ to 15°. There was virtually no change in B at $P/D = 1.25$ (Fig. 11(a)). Also, for very small incidence angles, in the nearly tandem configuration, a zero lift force is now experienced from $\alpha = 0^\circ$ to 6° (Fig. 10(a)). Overall, the effects of shear on the upstream cylinder are small when the cylinders are nearly tandem, with the critical incidence angles shifting by only a few degrees. This small change is similar to the small movement of the stagnation, maximum-velocity, and separation points for a single, isolated circular cylinder in a low-to-moderate planar shear flow (Akosile, 2002; Sumner and Akosile, 2002).

4.2. Forces on the downstream cylinder

For the downstream cylinder (Figs. 10(b) and 11(b)), the mean drag coefficient is the force component more strongly affected by the uniform planar shear flow. The shear flow causes a reduction in the drag coefficient similar to what was observed for the upstream cylinder, however the drag coefficient remains unchanged at smaller incidence angles, $\alpha < 30-35^\circ$, when the inner shear layer from the upstream cylinder wraps around, or reattaches onto, the downstream cylinder (Fig. 5). At higher incidence angles, however, when there is flow directed through the gap between the cylinders (Fig. 5), there is a drag coefficient reduction of similar magnitude to the upstream cylinder, with a more pronounced reduction when $U_{C,d} > U_{C,u}$ (Fig. 2(b)).

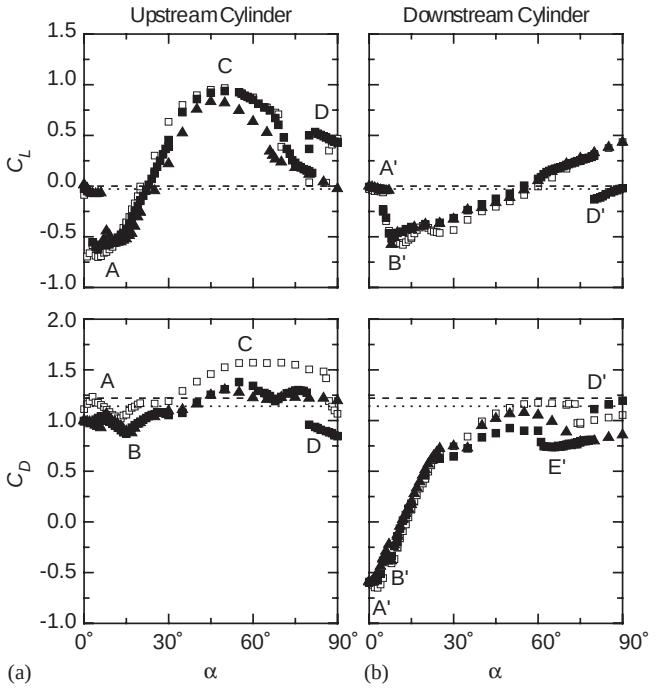

Fig. 10. Aerodynamic force coefficients for a staggered configuration of $P/D = 1.125$ in a uniform planar shear flow, $K = 0.05$, $\mathrm{Re} = 5.0 \times 10^4$: (a) upstream cylinder; (b) downstream cylinder. ■, $U_{C,d} > U_{C,u}$; ▲, $U_{C,d} < U_{C,u}$; □, no shear, $K = 0$. Single, isolated circular cylinder: ---, no shear, $K = 0$, $\mathrm{Re} = 5.0 \times 10^4$; …, with shear, $K = 0.05$, $\mathrm{Re} = 5.0 \times 10^4$.

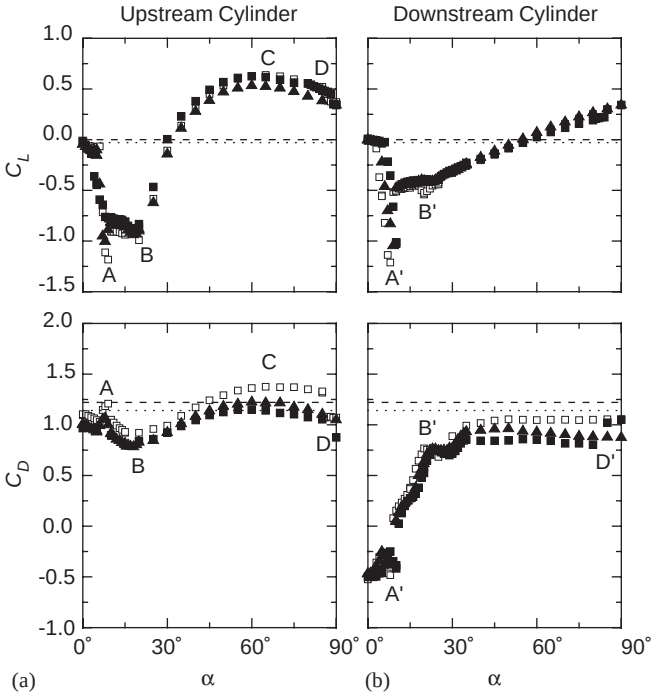

Fig. 11. Aerodynamic force coefficients for a staggered configuration of $P/D = 1.25$ in a uniform planar shear flow, $K = 0.05$, $\mathrm{Re} = 5.0 \times 10^4$: (a) upstream cylinder; (b) downstream cylinder. ■, $U_{C,d} > U_{C,u}$; ▲, $U_{C,d} < U_{C,u}$; □, no shear, $K = 0$. Single, isolated circular cylinder: ---, no shear, $K = 0$, $\mathrm{Re} = 5.0 \times 10^4$; …, with shear, $K = 0.05$, $\mathrm{Re} = 5.0 \times 10^4$.

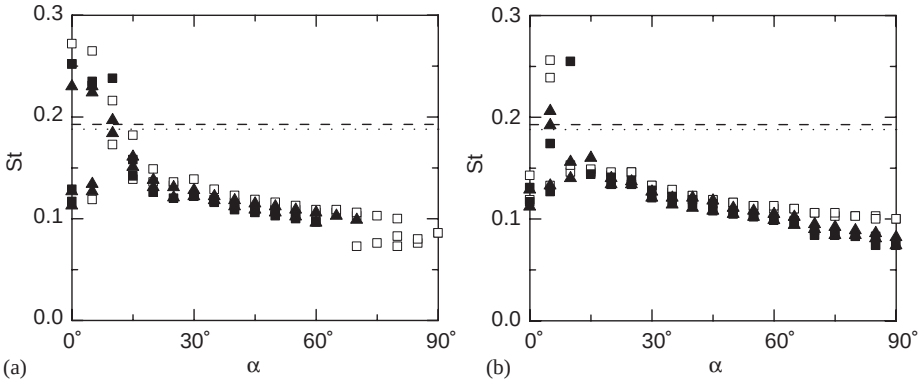

Fig. 12. Strouhal number data for staggered cylinders in a uniform planar shear flow, $K = 0.05$, $\mathrm{Re} = 5.0 \times 10^4$: (a) $P/D = 1.125$; (b) $P/D = 1.25$. ■, $U_{C,d} > U_{C,u}$, upstream and downstream cylinders; ▲, $U_{C,d} < U_{C,u}$, upstream and downstream cylinders; □, no shear, $K = 0$, upstream and downstream cylinders. Single, isolated circular cylinder: - - -, no shear, $K = 0$, $\mathrm{Re} = 5.0 \times 10^4$; …, with shear, $K = 0.05$, $\mathrm{Re} = 5.0 \times 10^4$.

Another effect of the shear flow is seen for $P/D = 1.125$ (Fig. 10(b)), where there is a shift in critical incidence angle E′ to a lower value of α. The shift is most pronounced for $U_{C,d} > U_{C,u}$, moving from $\alpha \approx 73^\circ$ to 60°, but also occurs for $U_{C,d} < U_{C,u}$. Critical incidence angle E′ was related to a sudden change in the direction of the gap flow, with the flow being directed towards the downstream cylinder at higher α. The effect of the sheared freestream, therefore, would be to initiate the direction change at a lower incidence angle.

The lift coefficient data for the downstream cylinder are mostly unchanged in the uniform planar shear flow (Figs. 10(b) and 11(b)). The location of the "inner lift peak" and critical incidence angles A and B shift by only a few degrees, and, the behaviour of the lift coefficient at smaller incidence angles is relatively unaffected. The major influence of the planar shear flow is seen at very high incidence angles, when the cylinders are nearly side-by-side, with the appearance of a new critical incidence angle, denoted D′, for $U_{C,d} > U_{C,u}$ only. Here, there is a sudden drop in the lift coefficient and a sudden rise in the drag coefficient with increasing α, which is most apparent at the smaller pitch ratio, $P/D = 1.125$ (Fig. 10(b)). This critical incidence angle coincides with new location of critical angle D identified for the upstream cylinder (Figs. 10(a) and 11(a)). The appearance of D′ means that the maximum outward-directed (positive) lift force experienced by the downstream cylinder no longer occurs in the side-by-side configuration (Fig. 10(b)). This pair of critical incidence angles, D and D′, was attributed to changes in the deflection or strength of the base-bleed flow.

4.3. Strouhal number

The Strouhal number data for staggered configurations of $P/D = 1.125$ and 1.25, in a uniform planar shear flow, are given in Fig. 12; selected power spectra of the velocity signals are given in Fig. 13. Since nearly the same Strouhal number was measured behind the upstream and downstream cylinders (see Fig. 8), no distinction between the two cylinders is given in Fig. 12.

At most incidence angles, the Strouhal number data are relatively unaffected by the presence of shear, although a small reduction of the Strouhal number may be discerned in Fig. 12. This small reduction is similar to what was observed for the single circular cylinder in a uniform planar shear flow at higher subcritical Reynolds numbers (Table 1), and therefore would be consistent with the closely spaced staggered cylinders behaving as a single bluff body. The lowering of the Strouhal number is quite pronounced at higher incidence angles, seen at $P/D = 1.25$ (Fig. 12(b)) for $\alpha > 60^\circ$. Also for $P/D = 1.25$, there is a reduction in the maximum attained value of the Strouhal number at $\alpha = 5-10^\circ$, from $\mathrm{St} \approx 0.26$ to 0.19, with the introduction of the shear flow; compare Figs. 8(b) and 12(b), and the power spectra in Figs. 9(b) and 13(b).

Many details of the power spectra, shown in Fig. 13, are largely unchanged from the no-shear case, with small, broad-banded or absent vortex shedding peaks at small incidence angles, $\alpha < 20^\circ$, for both $P/D = 1.125$ and 1.25, and particularly for the upstream cylinder.

For $P/D = 1.125$, the Strouhal number data (Fig. 12(a)) for $\alpha > 70^\circ$ were unreliable. Vortex shedding peaks were absent from the power spectra, as shown in Fig. 13(a). Within this same range of α are also found critical incidence angles D, D′ and E′ in the aerodynamic force data (Figs. 10 and 11), which are thought to be caused by changes in the deflection angle and strength of the gap flow. One of the effects of base bleed is to stabilize the wake, and under certain

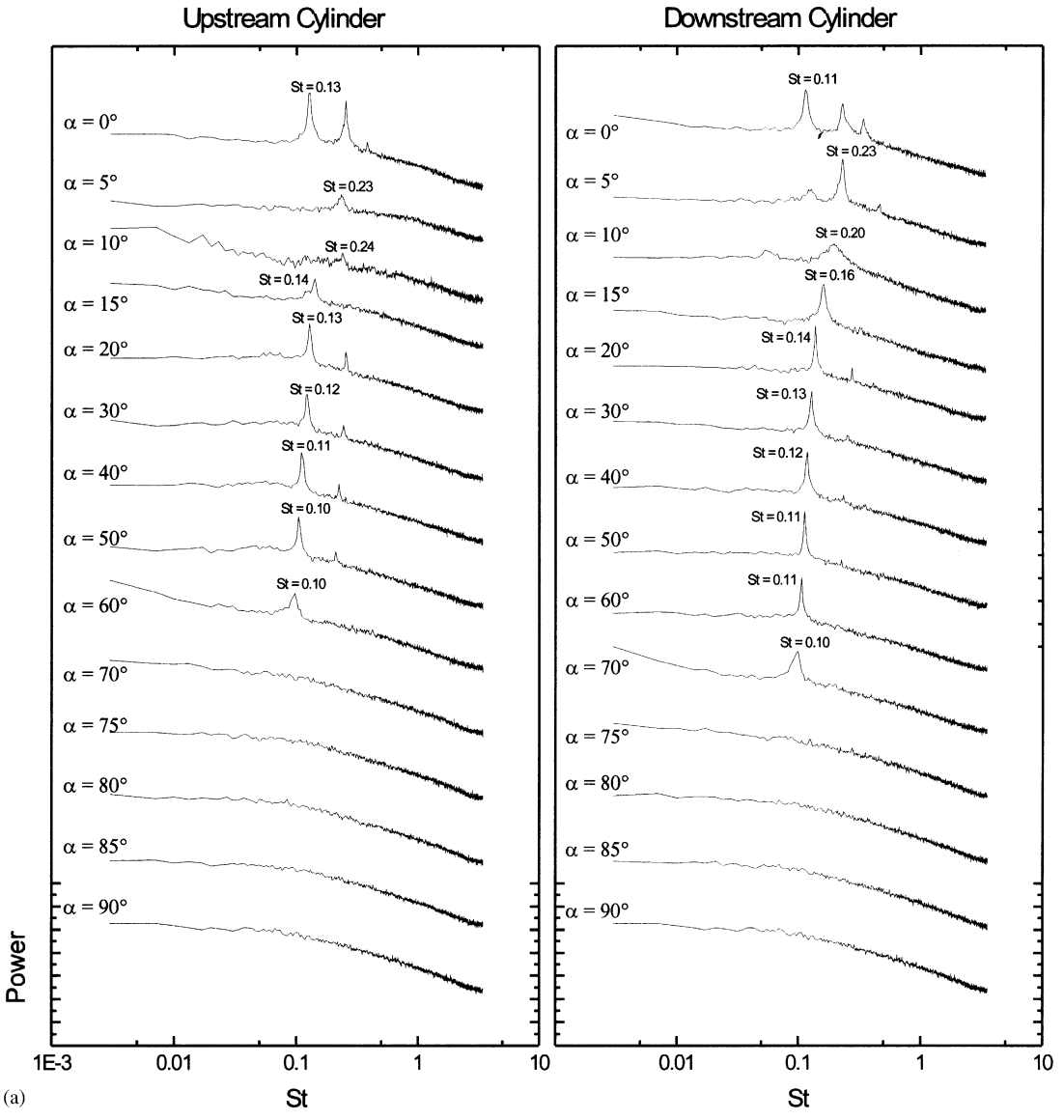

Fig. 13. Selected power spectra, as a function of incidence angle, measured behind the upstream and downstream cylinders, in a planar shear flow, $K = 0.05$, $\mathrm{Re} = 5.0 \times 10^4$, $U_{C,d} > U_{C,u}$, corresponding to the Strouhal number data in Fig. 12: (a) $P/D = 1.125$; (b) $P/D = 1.25$. Each spectrum represents 250 averages. The vertical scale is arbitrary, but the same scale is used for each spectrum.

conditions vortex shedding may be suppressed (Wood, 1967). Therefore, the absence of reliable Strouhal number data may have been caused by a change in the gap flow, such that the vortex shedding process becomes weakened, irregular, or even suppressed.

This absence of vortex shedding could also have been caused by a transition to turbulence, as in the critical flow regime for a single circular cylinder. The transition could have been aided by the elevated freestream turbulence intensity in the shear flow, which was 1.5% at the location of the cylinders, but it was not possible to verify transition from the present experiments. The literature pertaining to multiple cylinder experiments at very high subcritical Reynolds numbers, i.e. $\mathrm{Re} < 10^5$, and at elevated levels of freestream turbulence intensity, is inconclusive on this issue. Experimental data for closely spaced side-by-side cylinders ($\alpha = 90°$) at $\mathrm{Re} = 1.2 \times 10^5$–$2.4 \times 10^5$ from Quadflieg (1977) and Okajima et al. (1986), both reported in the review article by Ohya et al. (1989), and for staggered cylinders at high incidence angles at $\mathrm{Re} = 2.2 \times 10^5$–$3.3 \times 10^5$ by Gu and Sun (1999), do not indicate a suppression of vortex shedding or a transition to turbulence. However, different results are reported by Jendrzejczyk and Chen (1986), who examined two

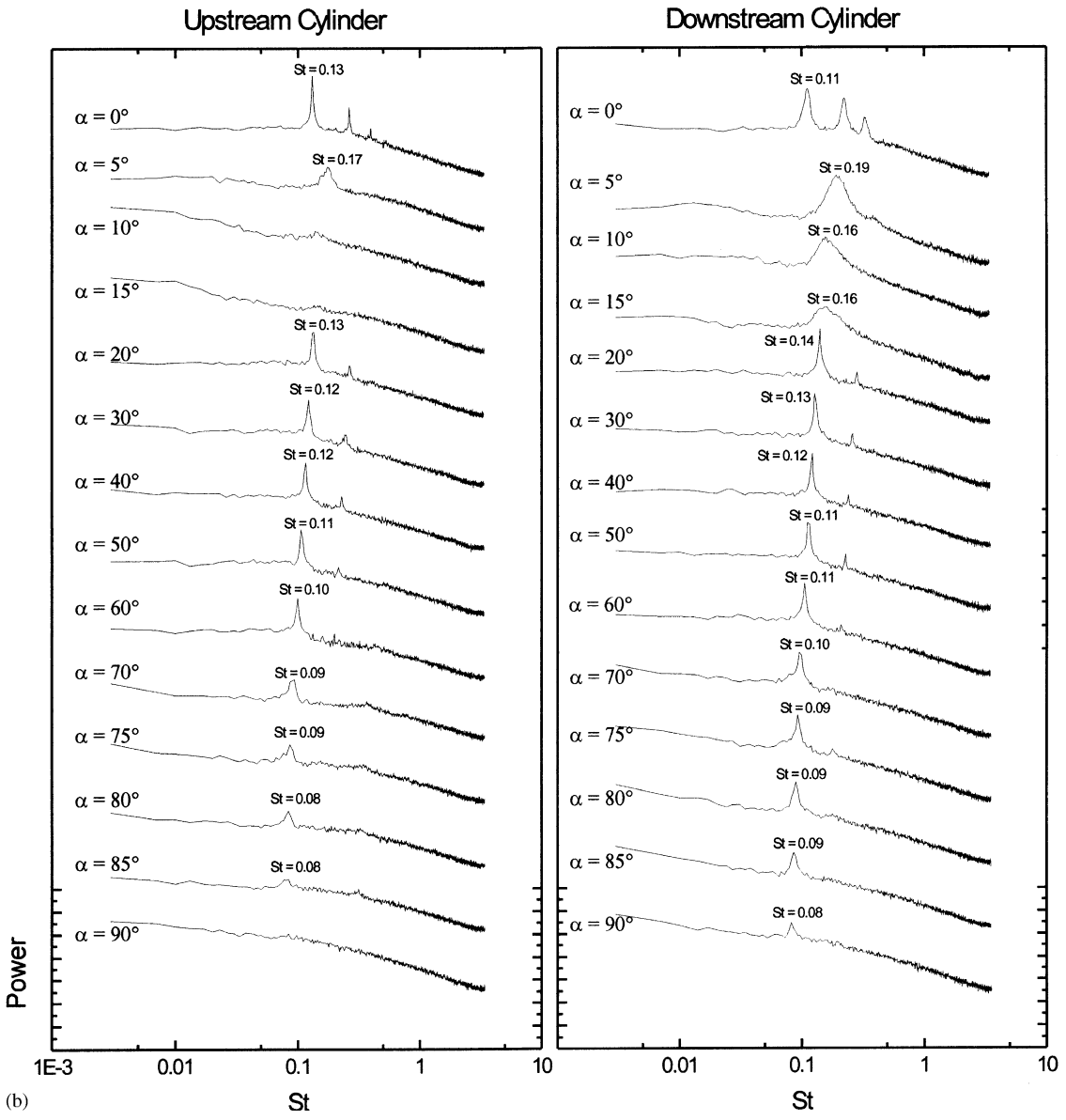

Fig. 13 (*continued*).

side-by-side cylinders at $P/D = 1.35$ in the high subcritical regime. Their results appear to show a suppression of vortex shedding from the two cylinders at $\mathrm{Re} = 8 \times 10^4$ when the turbulence intensity was raised from 1–3% to 4–5%. Their results also showed that the vortex shedding peak in the power spectra became less distinct and identifiable as Re was increased into the critical regime and at elevated turbulence intensity.

There is also a change in the power spectra for the $P/D = 1.25$ configuration, where the vortex shedding peaks for $\alpha > 70^\circ$ are smaller and more broad-banded than the case of uniform flow; compare Figs. 9(b) and 13(b). This suggests that vortex shedding from the cylinders has been weakened by the action of the uniform planar shear flow, through changes to the flow in the base regions of the cylinders, but it is not suppressed completely.

4.4. Further discussion

Overall, most of the important changes to the behaviour of the aerodynamic force coefficients, in a planar shear flow, occur at higher incidence angles, where the cylinders are closer to the side-by-side configuration. The shear flow

influences predominantly the behaviour of the flow through the gap between the cylinders, and the effect of base bleed, for closely spaced staggered configurations. At smaller incidence angles, the effects of the planar shear flow on the aerodynamic force coefficients are small or negligible, except for the upstream cylinder, which is more fully exposed to the incident shear flow. These small changes are consistent with the effects of shear on a single, isolated circular cylinder (Table 1; Akosile, 2002; Sumner and Akosile, 2002), which are themselves small.

Some of the changes to the force behaviour included a reduction in the drag coefficient, and the shift or movement of critical angles of incidence, which denoted discontinuous behaviour or extreme values of the drag and lift coefficients. The more closely spaced staggered configuration of $P/D = 1.125$ was more sensitive to the uniform planar shear flow, as was the case when the downstream cylinder was at a higher centre-line velocity than the upstream cylinder, i.e. $U_{C,d} > U_{C,u}$.

To obtain some further insight into the effects of shear flow, the total mean aerodynamic force (or resultant force) acting on each cylinder, represented by the dimensionless coefficient, $C_T (= (C_L^2 + C_D^2)^{1/2})$, and its direction with respect to the mean flow, $\theta (= \arctan(C_L/C_D))$, were calculated for $P/D = 1.125$, see Fig. 14. In a uniform flow, the resultant force on the upstream cylinder (Fig. 14(a)) is consistently greater than that experienced by a single, isolated circular cylinder, which indicates an unfavourable aerodynamic loading for this cylinder when arranged in close proximity to another cylinder. The direction of the force on the upstream cylinder is inward-directed at smaller incidence angles, $\alpha < 25^\circ$, and outward-directed at higher incidence angles, $\alpha > 25^\circ$. The resultant force on the downstream cylinder (Fig. 14(b)) is consistently lower than that experienced by a single, isolated circular cylinder, indicating that this cylinder experiences a favourable aerodynamic loading when located in a closely spaced staggered group. Its direction remains inward-directed except at high incidence angles, $\alpha > 60^\circ$.

The overall effect of the planar shear flow is to lower the magnitude of the total aerodynamic force on each cylinder (Fig. 14), which is similar to what is observed for a single, isolated circular cylinder. This reduction is more uniformly experienced with α for the upstream cylinder. For the downstream cylinder, the favourable effect of shear in lowering the aerodynamic force is particularly evident at the higher incidence angles. The effect of the relative centre-line velocities is different for the upstream and downstream cylinders, with the lowering of the resultant mean aerodynamic force on the downstream cylinder being more pronounced for $U_{C,d} > U_{C,u}$ (Fig. 14(b)).

In contrast, the direction of the resultant force, θ, is mostly unaffected by the introduction of shear (Fig. 14), apart from the changes in the critical incidence angles described earlier. This result is consistent with the effect of

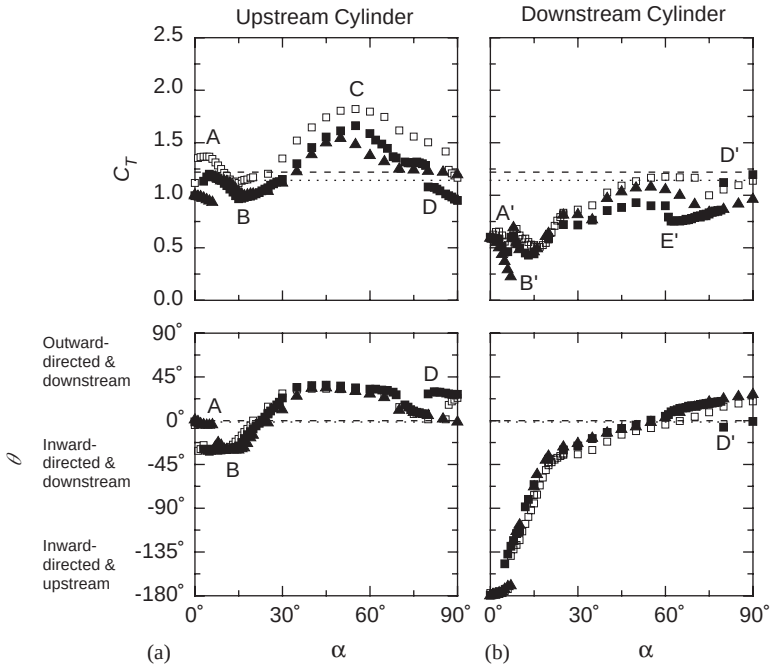

Fig. 14. Total aerodynamic force coefficient and its direction for a staggered configuration of $P/D = 1.125$ in a uniform planar shear flow, $K = 0.05$, $\mathrm{Re} = 5.0 \times 10^4$: (a) upstream cylinder; (b) downstream cylinder. ■, $U_{C,d} > U_{C,u}$; ▲, $U_{C,d} < U_{C,u}$; □, no shear, $K = 0$. Single, isolated circular cylinder: ---, no shear, $K = 0$, $\mathrm{Re} = 5.0 \times 10^4$; …, with shear, $K = 0.05$, $\mathrm{Re} = 5.0 \times 10^4$.

low-to-moderate shear on the single, isolated circular cylinder, in which the direction of the resultant force was changed by only 1.5° at $K = 0.05$ (Sumner and Akosile, 2002).

5. Conclusions

An experimental investigation was conducted of two closely spaced staggered circular cylinders of equal diameter, with $P/D = 1.125$ and 1.25, at $\mathrm{Re} = 5.0 \times 10^4$. The mean aerodynamic forces acting upon the cylinders, and the Strouhal numbers, were measured for two different approach flow conditions, namely uniform flow, $K = 0$, and a low-to-moderate uniform planar shear flow, $K = 0.05$.

Under no-shear conditions, $K = 0$, the mean aerodynamic force coefficients and the Strouhal number for each cylinder are considerably different from a single, isolated circular cylinder, as α is varied. The general behaviour of the forces and the vortex shedding frequency was similar for both pitch ratios, since the flow pattern for closely spaced staggered cylinders is similar to a single bluff body, with a single vortex shedding process. Several critical incidence angles were identified in the behaviour of the aerodynamic force coefficients with α. These were associated with extreme values of the lift or drag forces, or sudden changes or discontinuities in the lift and drag forces. At lower incidence angles, the critical angles were related to changes in shear layer dynamics from the inside of the upstream cylinder, as it wraps around, or reattaches onto, the downstream cylinder. At higher incidence angles, the critical angles were linked to changes in the deflection angle and the strength of the gap flow between the cylinders, as it entered the near-wake region of the cylinder pair, acting as a base bleed. The Strouhal number data were mostly identical for the upstream and downstream cylinders, again an indication of a single vortex street, and ranged from a Strouhal number higher than a single cylinder at small α, to a Strouhal number lower than a single cylinder at large α.

The effects of the low-to-moderate uniform planar shear flow, of $K = 0.05$, were mostly seen in the aerodynamic force data, and in particular the mean drag coefficient. For the upstream cylinder, a reduction in drag was measured at all incidence angles, whereas for the downstream cylinder drag reduction was observed only at higher incidence angles. The lift coefficient magnitude was mostly unchanged in the planar shear flow, for both cylinders, except for the movement of several of the critical points. In contrast to the aerodynamic force coefficients, the Strouhal number data were mostly unchanged from the no-shear case, with only a small overall reduction in Strouhal number. The reduction in drag, small changes to the lift forces, and small changes to the vortex shedding frequencies and power spectra, are consistent with the effects of shear on the single, isolated circular cylinder. This occurrence is not unexpected because the flow field for the closely spaced staggered cylinders is similar to that of a single bluff body, with a single vortex street.

Planar shear flow more strongly influenced the staggered cylinders when they were oriented at a high incidence angle. At higher incidence angles, the flow pattern is dominated by the flow through the gap between the cylinders, which enters the combined near-wake and acts as a base bleed. The shear flow had an influence on the direction and strength of the gap flow, which was seen in the movement of two critical incidence angles, with some sensitivity to whether the downstream cylinder experienced a higher or lower centre-line velocity than the upstream cylinder. There was also evidence, from the power spectra and Strouhal number data, that the shear flow acted to either suppress or weaken the vortex shedding process at high incidence angles. The shear flow had less of an influence on the staggered cylinders at lower incidence angles, where the shear layer from the upstream cylinder either wraps around or reattaches onto the downstream cylinder.

Acknowledgements

The support of the Natural Sciences and Engineering Research Council (NSERC) of Canada, the University of Saskatchewan President's NSERC Fund, and the Department of Mechanical Engineering, is gratefully acknowledged. The assistance of D. Braun, D. Deutscher, J.L. Heseltine, M.D. Richards, and Engineering Shops, is also appreciated.

References

Adachi, T., Kato, E., 1975. Study on the flow about a circular cylinder in shear flow. Journal of the Japan Society for Aeronautical and Space Sciences 23, 311–319 (in Japanese).

Akosile, O.O., 2002. Circular cylinders in a uniform planar shear flow. M.Sc. Thesis, Department of Mechanical Engineering, University of Saskatchewan, Canada.

Akosile, O.O., Sumner, D., 2001. Design of a shear flow generator for wind tunnel testing of circular cylinders. In: Swamidas, A., et al. (Eds.), Proceedings of the 18th Canadian Congress of Applied Mechanics. St. John's, Canada, pp. 363–364.

Bearman, P.W., 1967. The effect of base bleed on the flow behind a two-dimensional model with a blunt trailing edge. The Aeronautical Quarterly 18, 207–224.

Cooper, K.R., 1974. Wind tunnel measurements of the steady aerodynamics forces on a smooth circular cylinder immersed in the wake of an identical cylinder. National Research Council of Canada, LTR-LA-119.

El-Taher, R.M., 1984. Experimental study of the interaction between a pair of circular cylinders normal to a uniform shear flow. Journal of Wind Engineering and Industrial Aerodynamics 17, 117–132.

Griffin, O.M., 1985. Vortex shedding from bluff bodies in a shear flow: a review. ASME Journal of Fluids Engineering 107, 298–306.

Gu, Z.F., Sun, T.F., 1999. On interference between two circular cylinders in staggered arrangement at high subcritical Reynolds numbers. Journal of Wind Engineering and Industrial Aerodynamics 80, 287–309.

Hayashi, T., Yoshino, F., Waka, R., 1991. An analytical evaluation of the aerodynamic forces acting on a circular cylinder in a uniform shear flow. In: Morris, M.J., et al. (Eds.), Proceedings of the First ASME/JSME Fluids Engineering Conference, FED-Vol. 112. Portland, Oregon, pp. 83–88.

Hayashi, T., Yoshino, F., Waka, R., 1993. The aerodynamic characteristics of a circular cylinder with tangential blowing in uniform shear flows. JSME International Journal Series B 36, 101–112.

Jendrzejczyk, J.A., Chen, S.S., 1986. Fluid forces on two circular cylinders in cross-flow. In: Chen, S.S., Simonis, J.C., Shin, Y.S. (Eds.), Flow-Induced Vibration—1986, Chicago, Illinois, PVP-Vol. 104. ASME, New York, pp. 1–13.

Kiya, M., Arie, M., Tamura, H., 1979. Forces acting on circular cylinders placed in a turbulent plane mixing layer. Journal of Industrial Aerodynamics 5, 13–33.

Kiya, M., Arie, M., Tamura, H., Mori, H., 1980a. Vortex shedding from two circular cylinders in staggered arrangement. ASME Journal of Fluids Engineering 102, 166–173.

Kiya, M., Tamura, H., Arie, M., 1980b. Vortex shedding from a circular cylinder in moderate-Reynolds-number shear flow. Journal of Fluid Mechanics 141, 721–735.

Kotansky, D.R., 1966. The use of honeycomb for shear flow generation. AIAA Journal 4, 1490–1491.

Kwon, T.S., Sung, H.J., Hyun, J.M., 1992. Experimental investigation of uniform-shear flow past a circular cylinder. ASME Journal of Fluids Engineering 114, 457–460.

Ljungkrona, L., Norberg, C., Sundén, B., 1991. Free-stream turbulence and tube spacing effects on surface pressure fluctuations for two tubes in an in-line arrangement. Journal of Fluids and Structures 5, 701–727.

Ohya, Y.O., Okajima, A., Hayashi, M., 1989. Wake interference and vortex shedding. In: Cheremisinoff, N.P. (Ed.), Encyclopedia of Fluid Mechanics—Aerodynamics and Compressible Flow, Vol. 8. Gulf Publishing Company, Houston, pp. 322–389.

Okajima, A., Sugitani, K., Mizota, T., 1986. Flow around a pair of circular cylinders arranged side by side at high Reynolds numbers. Transactions of the JSME 52 (480), 2844–2850 (in Japanese), cited in Ohya et al. (1989).

Price, S.J., Sumner, D., Smith, J.G., Leong, K., Païdoussis, M.P., 2002. Flow visualization around a circular cylinder near to a plane wall. Journal of Fluids and Structures 16, 175–191.

Quadflieg, V.H., 1977. Vortex induced load on pair of cylinders in incompressible flow at high Reynolds number. Forschung im Ingenieurwesen 43, 9–18 (in German), cited in Ohya et al. (1989).

Sumner, D., Akosile, O.O., 2002. On a circular cylinder in a uniform planar shear flow at subcritical Reynolds number. In: Proceedings of the Fifth International Symposium on Fluid–Structure Interactions, Aeroelasticity, Flow-Induced Vibration & Noise, New Orleans, USA, Paper No. IMECE2002-32170. ASME, New York.

Sumner, D., Richards, M.D., 2002. A closer investigation of the mean aerodynamic forces for two staggered circular cylinders in cross-flow. In: Proceedings of the Fifth International Symposium on Fluid–Structure Interactions, Aeroelasticity, Flow-Induced Vibration & Noise, New Orleans, USA, Paper No. IMECE2002-32179. ASME, New York.

Sumner, D., Richards, M.D., 2003a. Some vortex shedding characteristics of the staggered configuration of circular cylinders. Journal of Fluids and Structures 17, 345–350.

Sumner, D., Richards, M.D., 2003b. Vortex shedding from two circular cylinders in a staggered arrangement. In: Proceedings of FEDSM'03, Fourth ASME/JSME Joint Fluids Engineering Conference, Honolulu, USA, FEDSM2003-45519, July 6–11, 2003.

Sumner, D., Wong, S.S.T., Price, S.J., Païdoussis, M.P., 1999. Fluid behaviour of side-by-side circular cylinders in steady cross-flow. Journal of Fluids and Structures 13, 309–338.

Sumner, D., Price, S.J., Païdoussis, M.P., 2000. Flow-pattern identification for two staggered circular cylinders in cross-flow. Journal of Fluid Mechanics 411, 263–303.

Szepessy, S., 1993. On the control of circular cylinder flow by end plates. European Journal of Mechanics B/Fluids 12, 217–244.

Wood, C.J., 1967. Visualization of an incompressible wake with base bleed. Journal of Fluid Mechanics 29, 259–272.

Zdravkovich, M.M., Pridden, D.L., 1977. Interference between two circular cylinders; series of unexpected discontinuities. Journal of Industrial Aerodynamics 2, 255–270.